



# Exploitation of sub-micron cavitation nuclei to enhance ultrasound-mediated transdermal transport and penetration of vaccines



Sunali Bhatnagar<sup>a,\*</sup>, James J. Kwan<sup>a</sup>, Apurva R. Shah<sup>a,b</sup>, Constantin-C Coussios<sup>a</sup>, Robert C. Carlisle<sup>a</sup>

<sup>a</sup> Institute of Biomedical Engineering, Department of Engineering Science, Oxford, OX3 7DQ, UK

<sup>b</sup> Department of Oncology, University of Oxford, Oxford, OX3 7DQ, UK

## ARTICLE INFO

### Article history:

Received 5 April 2016

Received in revised form 13 June 2016

Accepted 10 July 2016

Available online 12 July 2016

### Keywords:

Ultrasound

Immunisation

Ovalbumin

Transdermal delivery

## ABSTRACT

Inertial cavitation mediated by ultrasound has been previously shown to enable skin permeabilisation for transdermal drug and vaccine delivery, by sequentially applying the ultrasound then the therapeutic in liquid form on the skin surface. Using a novel hydrogel dosage form, we demonstrate that the use of sub-micron gas-stabilising polymeric nanoparticles (nanocups) to sustain and promote cavitation activity during simultaneous application of both drug and vaccine results in a significant enhancement of both the dose and penetration of a model vaccine, Ovalbumin (OVA), to depths of 500  $\mu\text{m}$  into porcine skin. The nanocups themselves exceeded the penetration depth of the vaccine (up to 700  $\mu\text{m}$ ) due to their small size and capacity to 'self-propel'. *In vivo* murine studies indicated that nanocup-assisted ultrasound transdermal vaccination achieved significantly ( $p < 0.05$ ) higher delivery doses without visible skin damage compared to the use of a chemical penetration enhancer. Transdermal OVA doses of up to 1  $\mu\text{g}$  were achieved in a single 90-second treatment, which was sufficient to trigger an antigen-specific immune response. Furthermore, ultrasound-assisted vaccine delivery in the presence of nanocups demonstrated substantially higher specific anti-OVA IgG antibody levels compared to other transdermal methods. Further optimisation can lead to a viable, safe and non-invasive delivery platform for vaccines with potential use in a primary care setting or personalized self-vaccination at home.

© 2016 Published by Elsevier B.V.

## 1. Introduction

High rates of infectious disease transmission from needle stick injuries have led to 500,000 deaths from Hep B worldwide in 2004 [1]. Additionally, the emotional trauma and pain associated with injections inhibit patient compliance [2]. Thus, increasing widespread recognition of the disadvantages associated with the use of needles has fuelled research toward non-invasive alternatives. In the context of immunisation, several safe alternative methods of achieving reliable and effective vaccination are under development. Transdermal immunisation (TI) systems in particular have garnered much attention because of the richly immune-cell-populated milieu beneath, ultimately eliciting effective immune responses in both systemic and mucosal compartments [3,4]. Such devices also bypass the hepatic/gastrointestinal metabolism that detrimentally alter immune response profile. This approach involves the application of devices that transiently permeabilise the stratum corneum (SC) in order to enable vaccine delivery. A range of technologies has been proposed and developed in order to overcome the barrier presented by the SC to achieve transcutaneous needle free vaccination, including ballistics-based gene gun devices [5],

microneedles [6], iontophoresis [7], chemical enhancers and ultrasound-mediated cavitation [8]. This last approach utilises the shockwaves and microstreaming created by the expansion and violent collapse of gas bubbles in response to ultrasound exposure and is particularly attractive because it can be achieved using safe, low-cost technology already widely available within healthcare settings [9].

The vast majority of studies exploring the use of ultrasound-mediated permeabilisation of the skin have demonstrated that inertial cavitation and related mechanisms are effective in increasing the permeability of the skin to drug and vaccine molecules of around 40 to 70 kDa [8]. Early studies did not use a cavitation nucleation agent, and involved pre-exposure of the skin to ultrasound followed by application of the therapeutic in liquid form on the skin [10–12]. Ultrasound was thus primarily used as a mechanism to enhance skin permeabilisation, rather than the active transport of the therapeutic across the stratum corneum. More recent studies have utilised a simultaneous treatment protocol, whereby through the simultaneous application of drug solution and ultrasound, a higher dose of the drug is driven deeper into the skin [8,10].

Recent work has shown that inertial cavitation nucleated by micron-sized talc particles can also promote the active transport of molecules through a tissue mimicking material (TMM) by simultaneous application of ultrasound and model vaccine [13]. Alternative cavitation nuclei candidates with more clinical translatability include microbubbles

\* Corresponding author: Institute of Biomedical Sciences, Department of Engineering Science, University of Oxford, Off Roosevelt Drive, OX3 7DQ, UK.  
E-mail address: [sunali.bhatnagar@eng.ox.ac.uk](mailto:sunali.bhatnagar@eng.ox.ac.uk) (S. Bhatnagar).

(widely used as ultrasound contrast agents) and micron sized particles [14]. However, these candidates are of limited utility for transdermal delivery due to their rapid depletion and destruction at the skin surface. Recently, nano-sized cavitation nuclei (nanocups) capable of instigating and promoting inertial cavitation at modest pressure amplitudes and frequencies have been developed [15,16]. These particles mediate sustained cavitation for many minutes, allowing durable exploitation of inertial cavitation mechanisms. Additionally, their size allows for higher concentrations of cavitation nuclei particles and therefore higher intensities of inertial cavitation in a given volume of dosage media.

Nanocups have recently demonstrated enhanced transport of intravenously delivered drugs into tumours [15]. The use of nano-cavitation nuclei in a transdermal delivery system offers exciting potential for vaccine delivery, because they can potentially not only be used to enhance skin permeability but also to mediate the active transport of therapeutics across the stratum corneum without depletion. Here we seek to demonstrate the utility of nanocups for enhanced ultrasound-mediated transdermal vaccine delivery, by embedding them alongside (but not chemically bound to) a model vaccine in a hydrogel formulation that can also serve as a novel dosage form. This approach enables simultaneous application of ultrasound-mediated cavitation with the model vaccine, making it possible to explore the impact of nanoscale cavitation events on both skin permeability and active transport of the therapeutic both *ex vivo* and *in vivo*.

## 2. Methods and materials

### 2.1. *Ex vivo* skin source

Porcine skin was chosen as a model for human skin based on its similarities to human skin in terms of structure, thickness and cellular composition [17]. Furthermore, it has similar characteristic impedance ensuring comparable transmission of ultrasound into the skin [18,19]. Experiments were performed on full thickness porcine skin harvested from the medial thigh of the animals immediately after abattoir sacrifice (female Landrace pigs, weighing 40–50 kg). Hair on the surface of the skin was trimmed. Shaving and the use of hair removal chemicals were not performed to prevent affecting the integrity of the SC. Skin was then cut into smaller (50 × 50 mm) pieces, wrapped in aluminium foil and stored in a 4 °C fridge for no longer than 3 days. Prior to an experiment, skin was mounted in a Franz diffusion cell shown in Supplementary Fig. S1.

### 2.2. Nanocup (NC) cavitation nuclei formulation and characterisation

Nanocups (NCs) are gas-stabilising solid ‘cup’ shaped polymeric nanoparticles [15]. Briefly they are manufactured in a seed polymerisation reaction and are composed of a copolymer of hydroxyethylmethacrylate (HEMA) and methyl methacrylate (MMA) formed around and linked to a poly(styrene-co-divinylbenzene) (PS:DVB) copolymer core (10:1:6 v/v/v ratio of MMA:HEMA:DVB formed around a 300 nm diameter PS bead). Dynamic light scattering measured the diameter of NCs to be 460 nm ± 24 nm and the zeta potential as -15 mV ± 1 mV (n = 10).

### 2.3. *Ex vivo* coupling gel formulation

Before formulation within an ultrasound coupling gel [20], model vaccine and NCs were fluorescently labelled to enable tracking of their delivery through the skin. OVA (A5503, Sigma-Aldrich, UK) was conjugated with FITC dye using the Fluorotag FITC conjugation kit (FITC1, Sigma-Aldrich, UK). FITC-OVA was then added to each gel (±NC) at a concentration of 1.5 mg/mL in the gel. NC were labelled with anthracene, (excitation peak 362 nm (UV))/emission peak 407 nm (blue), to give fluorescent nanocups (F-NCs), and were added to the FITC-OVA laden gel at a concentration of 5 × 10<sup>9</sup> NC/mL.

SDS PAGE, fluorescence spectroscopy (Luminescence Spectrometer LS 50B, Perkin Elmer, USA) and dynamic light scattering (Zetasizer Nano ZS, laser wavelength 633 nm; Malvern Instruments, UK) were employed to verify OVA stability before and after ultrasound exposure in the presence and absence of NCs.

### 2.4. Therapeutic ultrasound setup, exposure parameters and acoustic cavitation detection

A focused ultrasound (FUS) transducer operating at 256 kHz at pressure amplitudes not exceeding 1.5 MPa was used to initiate cavitation in the coupling gel formulation. The FUS system is shown in Supplementary Fig. S1, and described in the legend to Supplementary Fig. S1 and in Ref. [13]. Acoustic emissions associated with acoustic cavitation were recorded throughout exposure using a 5 MHz passive cavitation detector confocally and co-axially aligned with the FUS transducer [20].

### 2.5. Electrical resistivity measurement

The comparison of the electrical conductivity of the skin is the current gold standard in detection and monitoring of skin permeability *in vitro* [21]. In order to determine permeability increases in the skin as a result of each treatment condition, the electrical resistance of the skin was used to determine conductivity enhancement ratios, as described in Tezel et al. [22]. Measurements were taken with PBS in both the donor and receiver compartments prior to and immediately following each treatment [23].

### 2.6. Multi-photon microscopy

Skin samples were imaged using multi-photon microscopy (MPM) to assess penetration of fluorescently labelled OVA and NCs. Immediately following ultrasound exposure, the treated skin samples were coated with fluorescent red 2 µm diameter latex beads (SpheroTech, USA) to demarcate the skin surface. These 2 µm beads were chosen because they were too large to diffuse through the skin. Thus the beads acted as markers for the skin surface to allow visualisation and quantification of the penetration depths of both FITC-OVA and nanocups in the skin. A modified BioRad Radiance 2100 MP Multiphoton Microscope (Zeiss; Jena, Germany), was used for 3D imaging. Near infrared (NIR) laser beams (λ = 800 nm) were obtained from a tunable 76 MHz femtosecond pulsed Ti:sapphire laser (Mira 900-F, Coherent, Ely, UK) pumped by a 10 W multiline argon ion laser (Verdi; Coherent). A Nikon S Fluor 20× objective (NA = 0.75) was used for all images. The emission wavelengths of the filters selected were: 495 nm (blue), 525 nm (green), and 595 nm (red). 3 dimensional, 3 colour images were obtained of XY dimension 389 × 389 µm up to 1.5 mm deep (z-slice resolution 1.95 µm) into each skin sample. 3D representations were generated from the data acquired using Imaris software (Bitplane, USA). Data was post processed using Matlab software (Mathworks, USA). A custom written algorithm obtained an extrapolated skin surface from the red beads, and then measured the depths in each column of the 3D image between this skin surface and every voxel containing FITC-OVA (stained green) or F-NC (stained blue) to obtain a distribution of depths. The depth distribution was weighted according to the fluorescence intensity of each voxel analysed, with a view to giving the intensity distribution of the FITC-OVA and F-NCs in each measured area of the skin. Positive control samples were not imaged due to the denaturation of FITC-OVA by sodium dodecyl sulphate (SDS), rendering it non-fluorescent.

### 2.7. *In vivo* study design

Studies were performed in line with UK Home Office legislation. 40 five-week-old BALB/c female mice were obtained from the Biomedical Services Unit at the John Radcliffe Hospital (Oxford, UK). Mice were divided into two 20 mice treatment groups consisting of a Delivery and

Distribution (DD) arm and an Immune Response (IR) arm (Supplementary Fig. S2). The purpose of the DD arm was to examine the penetration depth and dose of labelled FITC-OVA and F-NCs into murine skin immediately after treatment, therefore these mice were culled immediately after treatment. Mice in the IR arm of the study were examined for the provocation of an immune response as a result of OVA treatment after 14 days. Blood samples were taken before treatment, and 30 min after treatment and on days 14 and 35 of the study for detection of anti-OVA antibodies. In response to the absence of a detectable response at day 14, a booster treatment was performed on day 21 with increased concentrations of CpG and OVA (Supplementary Fig. S3). Individual experimental groups are outlined in Supplementary Table 1.

## 2.8. Coupling preparation

FITC-CpG and unlabelled CpG were obtained from Source Biosciences (Nottingham, UK) and reconstituted in sterile PBS. Coupling gel was prepared as described except a concentration of 2% was used to maintain viscosity post-addition of NC and OVA solutions. Deionised filtered water was added to control gel formulations, i.e. those that did not contain FITC-OVA or F-NCs, to ensure equivalent viscosity. The OVA concentration in all of the formulated gels used on day 0 of each study was 1 mg/mL. OVA and NCs used in the immune response study were untagged to prevent the presence of the dyes affecting the immune response. For the booster treatment, lower viscosity gel (0.5%) and higher OVA (2.5 mg/mL) and CpG dose (30 µg) were used to increase the possibility of measureable anti-OVA antibody in blood samples. Gel recipes for each study arm and treatment are shown in Supplementary Table 2.

## 2.9. In vivo ultrasound setup

A 9 cm<sup>2</sup> area at the side of the mouse abdomen was shaved and depilated 24 h prior to treatment to allow hair removal for effective sealing of the donor compartment, and time for the skin barrier to recover from the depilatory treatment. Immediately prior to treatment, the mice were sedated with 2% isoflurane and 98% oxygen (flow rate: 2 L/min) and the donor compartment was placed onto the skin surface. 4 mL of the coupling gel formulation was filled into the donor compartment and the transducer lowered down onto the mouse to allow for ultrasound transmission.

Mice in groups 3, 4 and 5 of the DD study, and groups 3 and 5 of the IR study were subjected to ultrasound treatment for 90 s. The ultrasound parameters were 256 kHz frequency, 1 MPa peak negative acoustic pressure, 10% duty cycle (10 ms on, 90 ms off) at a pulse repetition frequency of 10 Hz. The ultrasound field and focus position within the donor compartment remained identical to that in the *ex vivo* setup. Acoustic emissions were monitored with the same PCD setup in the *ex vivo* studies (data given in Supplementary Figs. S4 and S5).

## 2.10. Delivery and distribution study - determination of OVA dose in vivo

Murine skin was excised 6 min after treatment and flash frozen in liquid nitrogen. Prior to analysis by Enzyme-Linked Immunosorbent assay (ELISA), skin samples were defrosted and rinsed in ice-cold phosphate buffered saline (PBS) (Sigma-Aldrich, UK) to remove blood, and then weighed and homogenised. PBS was added to the samples at a concentration of 1 mL PBS/100 mg skin and homogenised on ice. The resulting suspension was sonicated on ice with an ultrasonic cell disruptor (Microson Ultrasonic cell disruptor, Misonix, NY, USA) and then centrifuged for 5 min at 5000 ×g. The supernatant was removed and stored at −20 °C until assay. An OVA Enzyme-linked immunosorbent assay (ELISA) kit (Agro Bio, Germany) was used to quantify levels of OVA in the tissue homogenate.

## 2.11. Delivery and distribution study - determination of histological damage in vivo

Skin sections from each group were fixed in formalin solution (10%, Product HT501128, Sigma Aldrich, UK) immediately after harvest. Alternate sections were mounted on slides and stained with H&E to detect skin damage. Slides were imaged on a Nikon Ti microscope (CFI S Fluor 40× objective, NA = 0.9).

## 2.12. Immune response study – determination of OVA-specific antibody response

Blood samples (20 µL) were taken from each mouse on day 0 (before treatment as a baseline), day 14 (for levels of anti-OVA antibody produced in response to treatment 1) and day 35 (response to booster treatment). Blood was diluted in 180 µL PBS (1:10 dilution) and centrifuged for 3 min at 3000 rpm. Supernatant was removed and frozen at −20 °C prior to analysis.

For ELISA, OVA was diluted to 1 µg/mL and 50 µL of this solution was added to each well of a Nunc-Immuno Maxisorb flat-bottom 96-well plate (Fisher Scientific, UK). The plate was sealed and incubated overnight at 4 °C. The plate was washed with PBS-Tween (0.5%) 6 times then blocking performed (5% w/v bovine serum albumin, 50 µL, 1 h, room temperature (RT)).

Serum samples (1:10 dilution) were diluted further for testing to 1:20 dilution in PBS and 50 µL was added to each well. Each sample was tested in triplicate and every experimental group contained serum from at least 3 ( $n \geq 3$ ) mice. The samples were sealed and incubated for 1.5 h at RT before the plate was washed (6 times, PBS-Tween). Goat anti-mouse IgG secondary antibody-HRP (Santa Cruz, USA) was diluted 1:5000 in PBS and 50 µL added to each well before 1 h incubation at RT. Following incubation, the plate was washed (6 times, PBS-Tween) and 50 µL of TMB substrate (80,091; Alpha Diagnostic International Inc., USA) was added to each well and left to develop at RT for 30 min. 50 µL of stop solution (80100; Alpha Diagnostics International Inc., USA) was added to each well. All ELISA plates were read at absorbance wavelength 450 nm on a FLUOstar Omega plate reader (BMG Labtech, Germany). The low level of the response generated prevented a dilution series titration being performed.

# 3. Results and discussion

## 3.1. Cavitation-enhanced *ex vivo* skin permeabilisation

The current gold standard in detection and monitoring of skin permeability *in vitro* is the measurement of electrical resistance of the skin before and after treatment: as skin is permeabilised, resistance decreases. NC in the absence of ultrasound did not change skin conductivity (Fig. 1A). Non-significant ( $p > 0.05$ ) changes were observed in the presence of ultrasound and NCs, both with and without OVA. Chemical permeabilisation using sodium dodecyl sulphate (SDS), in the absence of ultrasound, showed a significant (9.5-fold,  $p < 0.001$ ) increase in conductivity enhancement.

SDS has been widely studied as a chemical transdermal penetration enhancer because it is able to readily and reversibly disrupt the barrier properties of the skin, particularly the SC [24]. Notably, the most substantial (9.5-fold) increase in skin permeability in this study was observed upon exposure to SDS. However, the main disadvantage of the use of chemical penetration enhancers is skin irritation due to the damage they cause. In contrast, ultrasound exposure to the skin has not been observed to cause such damage. Consequently, assuming a suitable delivery profile is achievable with the small but observable permeability change associated with ultrasound skin treatment with NC-gel (either as a pre-treatment or simultaneously applied with the vaccine), this is a preferable option to the chemical penetration enhancer.

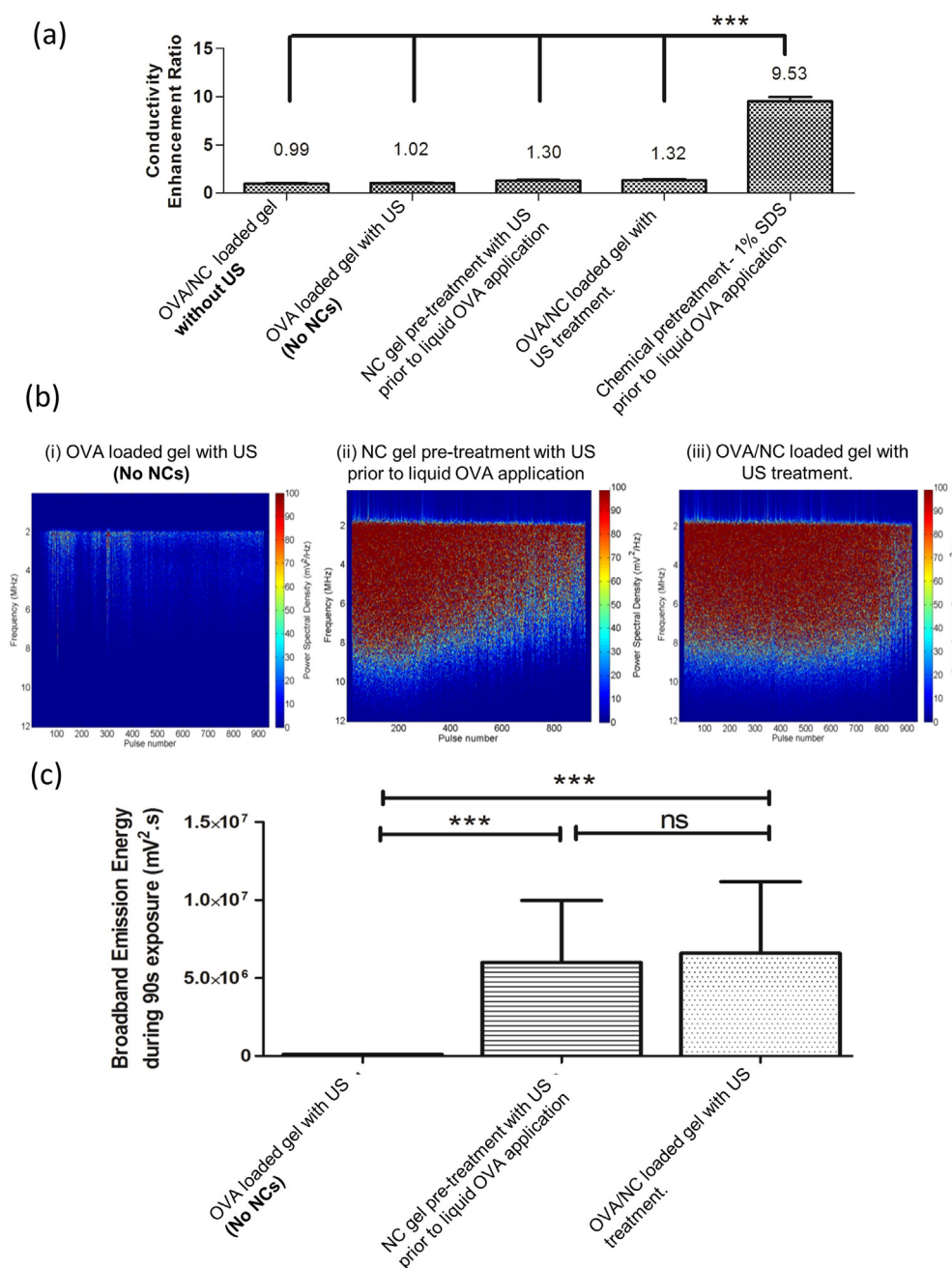


**Fig. 1.** (A) Skin conductivity enhancement ratios for each treatment regime. Average values are shown above each data bar. (B) Representative frequency spectrograms of the magnitude and temporal distribution of broadband acoustic emissions, as detected by the PCD in the coupling gel. (C) Total broadband energy emissions over the entire 90 s (900 pulse) exposure period, calculated as the sum of the integrals of the filtered Fourier Transforms for each pulse in the exposure.  $N = 3$ , standard deviations shown, \* denotes  $p < 0.05$ , \*\*\* denotes  $p < 0.005$ , using ANOVA with Bonferroni analysis to determine statistical differences between groups, n.s. = not significant.

Previous work has shown that the mechanisms responsible for ultrasound-mediated increases in skin permeability are more effective in the presence of inertial cavitation [25,26]. Therefore it follows that ultrasound coupling gels that favour inertial cavitation events due to the inclusion of cavitation nuclei will result in greater skin permeability. This effect was observed in the current study, where the acoustic emissions from the ultrasound focus during treatment were quantified and compared with increases in permeability. Spectrograms in Fig. 1B give a representation of the magnitude (represented by the colour-scale) and temporal (represented from left to right across the spectrogram) distribution of the frequency content of broadband acoustic emissions as exposures progress. Broadband emissions when the gel did not contain

any form of cavitation nuclei were sparse and of low magnitude (Fig. 1B(i)), whereas in the presence of NCs, broadband emissions from inertial cavitation were sustained and of high magnitude (Fig. 1B(ii) and (iii)). The average total emission energy over the exposure was also significantly lower in the absence of NCs ( $p < 0.001$ ) (Fig. 1C).

The increase in the magnitude of broadband emissions detected in the presence of NCs is due to nanobubbles on the NC surface [15], acting as nucleation sites that exclusively promote inertial cavitation [16]. Emissions were sustained due to repeated cavitation events per nanoparticle as well as their replenishment in the focus due to microstreaming currents set up in the gel. In the absence of NCs, inertial cavitation events were energetically more difficult to achieve [15].

### 3.2. Enhanced vaccine penetration ex vivo

MPM is a specialised fluorescence imaging technique that allows three dimensional imaging of biological tissue to penetration depths of the order of 1 mm. Skin sections were therefore imaged using MPM immediately after treatment with ultrasound to characterise the degree and depth of delivery of FITC-OVA and fluorescent NCs into the skin.

Fig. 2 shows qualitative and quantitative results for OVA and NC penetration in the four different treatment groups examined in this study. 3D image representations are shown in row (a) and give a summary of the difference in delivery for the four treatment conditions. In the absence of ultrasound treatment, OVA (green) and NCs (blue) penetrated the skin surface (red) very sparsely, and to a maximum depth of about 100  $\mu\text{m}$ . With the addition of ultrasound treatment but no NC, (Fig. 2A – application of OVA loaded gel with ultrasound (No NCs)) most of the drug dose was at the skin surface, with poor penetration beyond. Pre-treatment with NC in gel and ultrasound before OVA addition, showed minimal increase in OVA delivery, but considerable NC penetration, with penetration depths of up to 550  $\mu\text{m}$  (Fig. 2A – NC pre-treatment with ultrasound). Finally, when OVA was applied simultaneously with ultrasound and NCs in gel, OVA penetration depth increased substantially to 500  $\mu\text{m}$ , and OVA dose was also markedly increased. NCs in this group also penetrated to depths of 600–700  $\mu\text{m}$ .

Visual assessment of the MPM images enables qualitative comparison of delivery, but does not provide a quantitative assessment of the OVA and NC penetration achieved in each condition. For this purpose, Fig. 2B shows histograms of the depths measured for each fluorescent entity, weighted for pixel intensity to show concentration. Some autofluorescence of collagen was observed in the blue spectrum upon excitation with UV light (excitation/emission range: 270–370 nm/405–460 nm) [27]. To investigate the extent to which fluorescence emissions from collagen alone could be visualised in the skin at the microscopy settings used, the average pixel intensity and mean maximum penetration depth of the collagen in untreated skin samples was determined as  $8.56 \pm 2.04$  AU, and  $187.96 \pm 27.11$   $\mu\text{m}$  respectively. To prevent collagen signal being mistaken for NC signal, it was assumed that signal inside this intensity and depth in the blue channel could be collagen. This is represented on each distribution in Fig. 2B. These values were superimposed on the data and not subtracted because collagen fluorescence varies between skin samples, so subtraction of a mean value from all the samples was inappropriate.

OVA and NC penetration in the absence of ultrasound or NCs was sparse and shallow – reflected by low pixel intensity and poor (up to 150  $\mu\text{m}$ ) penetration depth, (Fig. 2B(i) and (ii)). Pre-treatment with ultrasound and NC-enriched gel resulted in separate distributions of OVA and NCs (Fig. 2B(iii)), because ultrasound pre-treatment with NC-

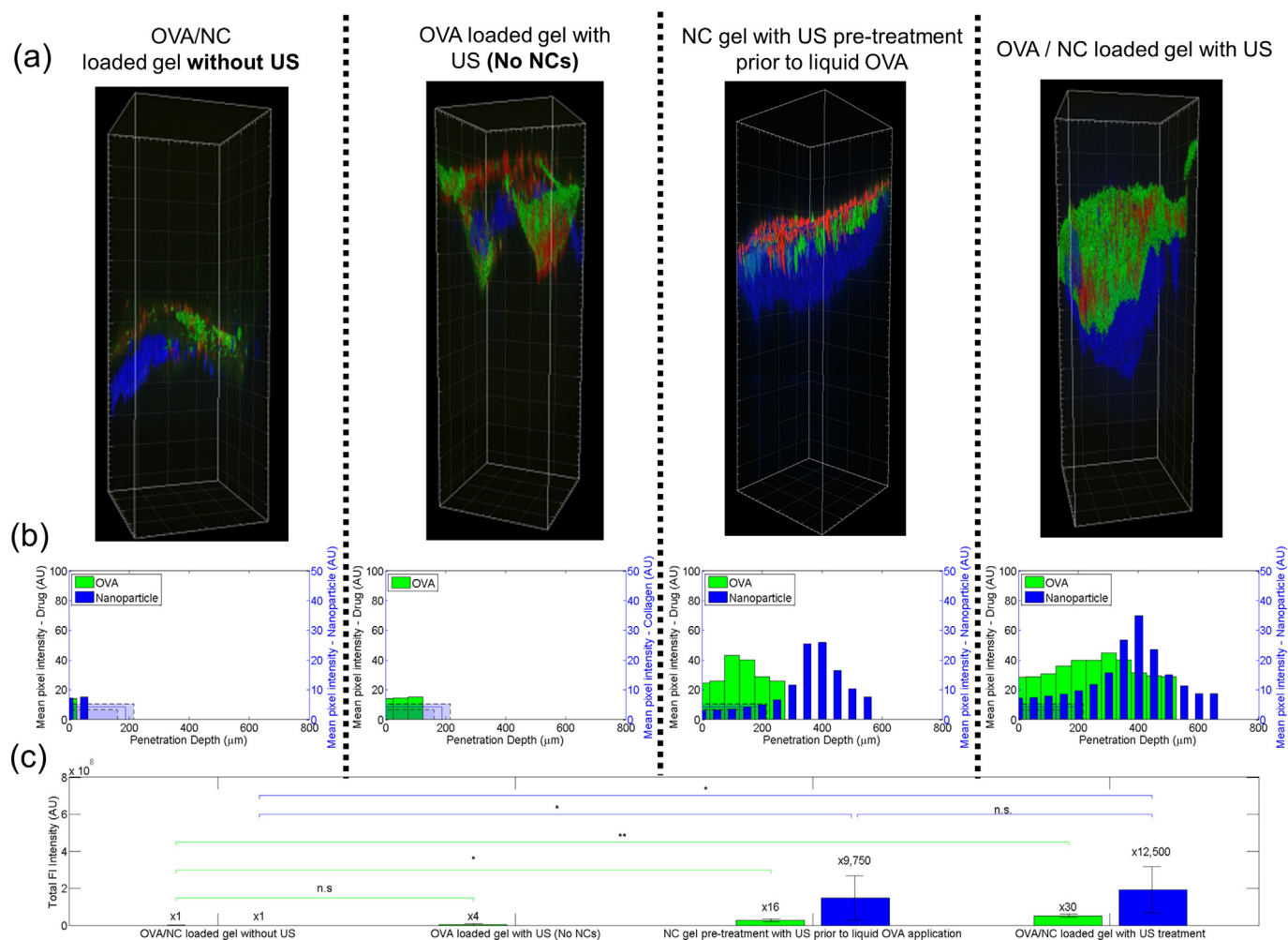


**Fig. 2.** (A) 3D visualisations of OVA and NC penetration in a single representative sample of each of the four visualised treatment groups. OVA = green, NCs = blue, and skin surface = red. Each square on the surrounding grid is 100  $\mu\text{m} \times 100 \mu\text{m}$ . Ultrasound exposure direction is vertically down through the images. (B) Quantitative OVA and NC distribution profiles for a single representative sample within each treatment group. Shaded regions represent mean  $\pm$  1SD of signal that may have originated from collagen in the skin rather than NCs. (C) Overall OVA and NC delivery doses for each treatment group, showing enhancements in dose delivery relative to the control (n = 3). ANOVA used to compare means \* indicates p < 0.05, \*\* indicates p < 0.01 and n.s. represents a non-significant result. (For interpretation of the references to colour in this figure legend, the reader is referred to the web version of this article.)

enriched gel enabled the NCs to penetrate and permeabilise the skin due to inertially collapsing bubbles on the NC surface. The penetration depth of liquid OVA applied after permeabilisation was also enhanced approximately 2-fold, but as OVA penetration was reliant on passive diffusion rather than cavitation-mediated active transport, it was not able to penetrate as deeply as the NCs, and the peak dose of OVA was seen at around 150  $\mu\text{m}$ , a distance insufficient to achieve marked interaction with Langerhans cells [28]. Simultaneous application of OVA with ultrasound and NCs enabled microstreaming mechanisms from inertial cavitation activity to provide an active transport mechanism for the OVA molecules. As a result, substantial dose enhancements (about 2-fold compared to the ultrasound pre-treatment group) were seen in the penetration depth of OVA when delivered simultaneously with ultrasound application in the presence of NC (Fig. 2C).

Both OVA and NCs showed markedly higher dose and penetration depth in the OVA/NC loaded gel with ultrasound treatment group than in the other three treatment groups (Fig. 2B(iv)). OVA dose peaked at 300  $\mu\text{m}$ , and the peak NC dose was at 400  $\mu\text{m}$ . Penetration depth of NCs was greater than OVA when ultrasound and cavitation related transport mechanisms were exploited. The NCs ability to propel themselves through tissue in an ultrasound field as a nanobubble repeatedly inertially cavitates on their surface is hypothesised to be responsible for this effect. Therefore, and in contrast to the OVA molecules, NC transport is not reliant upon only microstreaming from inertial cavitation. Such self-propulsion is not a mechanism applicable to microbubble formulations which are destroyed upon inertial cavitation instigation.

Overall OVA and NC dose was calculated as the sum of the intensities of all the green or blue fluorescent voxels in a 3D image stack (Fig. 2C). Significant enhancements in delivery were observed in both mean OVA and NC dose in the NC/OVA gel with ultrasound treatment group (OVA = 30-fold, NCs = 12,500-fold) compared to the application of OVA/NC gel without ultrasound, demonstrating enhanced delivery of both entities. With NC gel + US pre-treatment, the overall OVA concentration increased 16-fold compared to control, whilst with delivery where cavitation and OVA were concomitantly applied provided an increase of 30-fold relative to control. At first glance, it would thus seem that active transport during delivery only accounts for a further 2-fold increase over permeabilisation alone. However, it is worth noting that no OVA was delivered to depths >250  $\mu\text{m}$  in the pre-treatment group, whilst the increased concentration delivered by cavitation-enhanced transport reached depths of up to 550  $\mu\text{m}$ . Cells involved in immune response generation are found in the lower layers of the epidermis, at depths of around 200  $\mu\text{m}$  [28]. Even though there is still a significant advantage of cavitation-enhanced transport during delivery in terms of overall dose delivered, it is therefore most transformative in terms of mediating a previously unachievable penetration depth. NC dose and delivery profile in the cavitation-enhanced ultrasound pre-treatment group was similar to that seen in the simultaneous OVA/NC gel with ultrasound treatment group, as from the point of the NCs, they had seen the same ultrasound conditions and were unaffected by the application of the OVA.

### 3.3. Nano-nucleated cavitation enhanced transdermal delivery OVA dose *in vivo*

To determine the transdermal vaccine dose *in vivo*, the ultrasound-assisted system was modified and implemented in BALB/C mice (Supplementary Fig. S1), using OVA as a model vaccine and the same F-NCs used in the *ex vivo* study. Immediately following treatment, mice were sacrificed and skin from the treatment area excised. Sandwich ELISA was used to determine the OVA content in the skin homogenate.

In order to remove excess OVA and avoid artificially high readings, mouse skin was wiped with a damp paper towel after treatment. Fig. 3 shows the average OVA dose delivered to the skin per 90 s treatment. The dose delivered to the skin was zero in the group that contained no OVA, confirming the reliability of the assay. Application of the gel to the

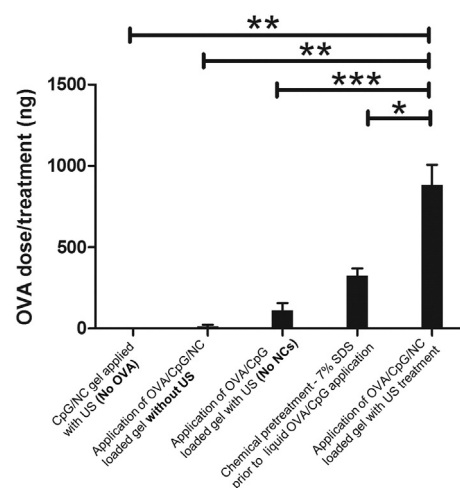


Fig. 3. OVA dose delivered following 90 s exposure to the skin of BalbC mice. Gel and exposure conditions as described on x-axis, \*, \*\* and \*\*\* represent p values of <0.05, 0.01 and 0.001 respectively using a one way ANOVA with Bonferroni multiple comparisons tests. n = 4 for each group except the CpG and gel with ultrasound (No OVA) group, where n = 2.

skin in the absence of ultrasound showed negligible delivery ( $8.79 \pm 24$  ng), that was not statistically different to the no OVA group. Upon the application of ultrasound but in the absence of cavitation inducing NC, OVA delivery increased to  $108 \pm 107$  ng, but once again this result was not statistically different to either of the two previously described groups. The addition of chemical penetration enhancer pre-treatment increased delivered dose approximately 3-fold, but delivery was highest ( $0.887 \pm 0.258$   $\mu\text{g}$ ) in the ultrasound/NC assisted vaccine delivery group, which was substantially (3-fold) and statistically ( $p < 0.05$ ) higher than the chemical penetration enhancer group, as well as every other group tested. Supplementary Fig. S4 shows acoustic emissions as measured by the PCD for each treatment, and results suggest that delivery was related to inertial cavitation levels during treatment.

Alternative transdermal vaccine delivery methods have shown similar vaccine delivery doses. In a dose sparing OVA study using microneedles in mice, specific antibody titers from microneedles after low dose (1  $\mu\text{g}$ ) application were one order of magnitude greater than subcutaneous injection and two orders of magnitude greater than intramuscular injection [29], indicating that transdermal delivery of a vaccine may represent a more efficient delivery route in terms of elicitation of a specific immune response for a given vaccine dose. The use of ultrasound specifically as a pretreatment was investigated in a previous *in vivo* study showing transdermal delivery of tetanus toxoid vaccine using low frequency (40 kHz) ultrasound as a pre-treatment prior to the application of a vaccine loaded patch. However a 2 h pre-treatment exposure was required in this study to deliver a dose of 1.3  $\mu\text{g}$ . Notably, this approach did generate an immune response comparable to that induced by a 10  $\mu\text{g}$  subcutaneous injection [23], again suggesting the efficiency of the transdermal route over subcutaneous injection.

### 3.4. Ultrasound-assisted vaccination causes no visible skin damage *in vivo*

In any proposed transdermal treatment application, the treatment must not cause irreversible or functional damage to the skin surface to the point where it is unable to protect the body from incoming pathogens. SC integrity was therefore assessed after each treatment *in vivo*. Possible causes of skin damage in this experiment included (1) damage caused by mechanical mechanisms from ultrasound exposure and inertial cavitation, or (2) chemical disruption from agents in the gels or skin pre-treatment. Fig. 4 shows cross sectional histological sections of

treated skin stained with hematoxylin and eosin (H&E) stain to enable visualisation of the different skin layers and structures within them. Panel (a) shows non-treated skin with SC intact and the epidermis and dermis clearly demarcated for comparison.

Assessment of the damage caused by ultrasound exposure can be performed by comparing images in panels (c) and (e) to panel (a). Panel (c) (without ultrasound exposure) shows negligible disruption. The lack of obvious difference between panels (c) and (e), indicates that ultrasound application did not cause structural damage to the SC, even in the presence of NC mediated inertial cavitation (Fig. 4E).

Among the currently used transdermal permeability enhancement modalities, chemical penetration enhancers are known for causing irritation and damage to the skin when used at concentrations exceeding 1–2% w/v. Chemical permeability enhancement is usually performed with the aim of reducing the barrier properties of the SC, and despite being reversible in most cases, causes vulnerability to external pathogens. Healing time from such chemical insult can also take several days, leaving the skin vulnerable for a considerable amount of time [30]. Substantial chemically induced damage to the SC was observed in this study (Fig. 4F, arrows). Application of SDS to the skin as a pre-treatment resulted in SC breakdown to the point where it was no longer attached to the skin, and in some cases, epidermal detachment occurred (shown by arrows, Fig. 4F) and marked redness and skin disruption was present on visual inspection prior to sacrifice. SDS concentration in this study was 7%, increased in from 1% (w/v) in the *ex vivo* study because as well as quantifying the skin damage occurred, the intent was also to identify the maximum OVA penetration possible in the presence of major to complete SC disruption. Non ablative ultrasound application at the parameters selected appeared to do no damage to the SC and resulted in the desired short-term disruption necessary for transdermal vaccine delivery.

### 3.5. OVA-specific antibody response from NC-nucleated inertial cavitation-enhanced transdermal delivery

The aim of the long term *in vivo* study was to elicit an OVA-specific antibody response with the nano-nucleated cavitation-assisted transdermal vaccine delivery system. Antibody response was assessed by a comparison of the levels of specific anti-OVA IgG antibodies in mouse blood before treatment *versus* after a prime-boost vaccination regimen. A vaccine boost was administered on day 21 of the study, with a higher OVA concentration (2.5 mg/mL vs. 1 mg/mL), a higher CpG dose (30 µg/mouse vs. 10 µg/mouse) compared to the primer treatment. Blood was taken on day 35 to examine anti-OVA antibody levels. A sandwich ELISA technique was used to quantify levels of anti-OVA IgG in the day 35 serum samples, and average absorbance readings ( $n = 4$ ) for each treatment group are shown in Fig. 5. In the absence of OVA and/or ultrasound, there were no significant differences in antibody levels compared to the pre-bleed (non-treated) mice, in accordance with negligible delivery measured in Fig. 3. Only the chemical penetration enhancement, the ultrasound-NC assisted transdermal vaccination, and the subcutaneous injection groups showed significantly different antibody levels to the pre-bleed mice, demonstrating the delivery measured in Fig. 3 could generate an immune response. In this study, subcutaneous injection was used as the positive control, and illustrates the antibody response at 100% dose delivery. Notably, the ultrasound/NC assisted system outperformed the chemical penetration enhancer group.

### 3.6. Future system development

The present work represents a proof-of-concept study that demonstrates the potential utility of ultrasound-mediated skin permeabilisation and molecular transport for transdermal vaccine

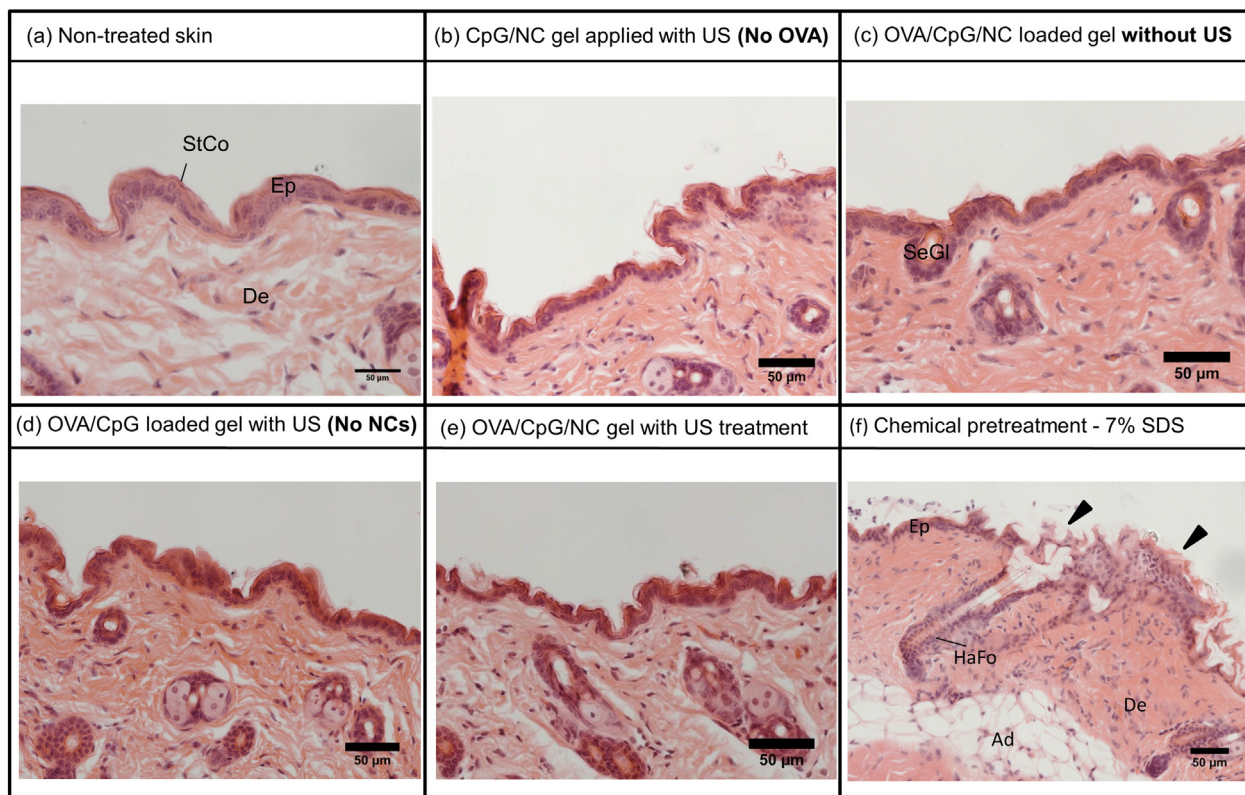


**Fig. 4.** Cross sectional images of Haemotoxylin and Eosin stained histological slides of murine skin after each of the treatment regimens tested. In all images, ultrasound was applied from the top downwards onto the skin surface. Key: StCo = stratum corneum, Ep = epidermis, De = dermis, Ad = adipose tissue, HaFo = hair follicle, SeGl = sebaceous gland. (Left) Comparison of epidermal thicknesses between treatment groups. \*\*\* and \*\* represent  $p < 0.001$  and  $p < 0.01$  respectively in one way ANOVA.

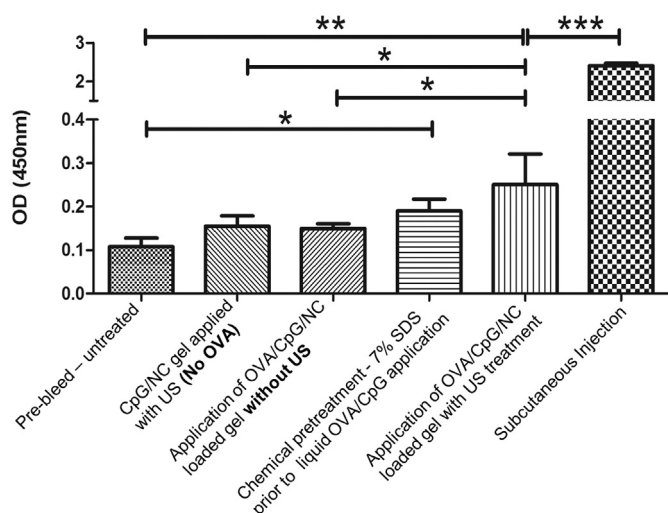


**Fig. 5.** Anti-OVA IgG antibody levels in all of the treatment groups on day 35 of the study. Mice were bled and serum diluted in PBS before being applied to a Nunc Maxisorp 96 well plate for analysis using a standard anti-OVA ELISA technique as described in methods. OD = optical density (absorbance).  $n = 4$ , standard deviation shown, significant differences determined by one-way ANOVA Bonferroni multiple comparison tests. \*\*\*, \*\* and \* =  $p < 0.05$ ,  $0.01$ ,  $0.001$  respectively.

delivery. Before this technology can begin to replace injections as the route of delivery in a clinical setting, further development and optimisation is necessary.

Firstly, vaccine stability for each different vaccine candidate must be assessed following ultrasound exposure, to ensure that vaccine structure and function is not adversely affected. In the present work, methods such as SDS PAGE, fluorescence spectroscopy and ELISA were employed to verify OVA stability before and after ultrasound exposure in the presence and absence of NCs. OVA structure and function were unchanged at the ultrasound parameters tested (Supplementary Fig. S6).

Despite achieving a significantly higher anti-OVA antibody level than the controls *in vivo*, the system presented in the current work was not able to illicit an immune response similar to that achieved by subcutaneous injection, which is the current gold standard. This is largely due to the low delivery efficiency associated to this not fully optimised delivery system, compared to 100% subcutaneous delivery resulting from injection. Increases in delivery dose and efficiency could be achieved by the optimisation of ultrasound parameters such as exposure time and pulse repetition frequency, to maximally exploit the NC cavitation nuclei and their instigation of inertial cavitation. Further optimisation strategies could include redesign of the ultrasound transducer to increase treatment area, decreasing the thickness of the vaccine dosage gel layer over the skin to allow the maximal dose of vaccine to lie directly above the skin and be ready for molecular transport, and conjugation of OVA/vaccine to the NCs so that propulsion of the NCs carry larger doses of the vaccine deeper into the skin.

#### 4. Conclusions

Inertial cavitation mediated by ultrasound has been previously shown to mediate permeabilisation of the skin surface to enhance the transdermal delivery of drugs and vaccines [8,31–34], typically by first exposing the skin to ultrasound and then applying the therapeutic on the skin in liquid form. In the present work, we demonstrate that the use of sub-micron cavitation nuclei to promote and sustain cavitation activity during simultaneous application of ultrasound and vaccine can significantly enhance both the dose and penetration of a therapeutic across the skin. This was achieved through the development of a novel dosage form, namely a hydrogel containing both cavitation-inducing

nanocups and the vaccine, which can also be used as a matching layer between the transducer and the skin.

Three regimes were initially tested *ex vivo* using porcine skin and ovalbumin (OVA) as a model vaccine. Embedding nanocups (but not OVA) into the hydrogel and exposing the skin to 90 s of ultrasound, followed by application of OVA in liquid form, enabled OVA to diffuse to an average depth of 150  $\mu\text{m}$  (Fig. 2b), with only a very small proportion detected at up to 250  $\mu\text{m}$ ; this result is comparable to previous studies which have sought to pre-permeabilize the SC by ultrasound [27–31]. These levels and depths of delivery are unlikely to provide an opportunity for substantial interaction with the Langerhans cells in the epidermis. Embedding both the cups and OVA in the hydrogel and exposing to 90 s of ultrasound resulted in the active transport of vaccine molecules to depths of up to 550  $\mu\text{m}$  into the skin, with cups reaching depths of 700  $\mu\text{m}$ . We thus hypothesise that microstreaming associated with the self-propelling nanocups enables them not only to permeabilize the stratum corneum but also to actively transport the co-administered therapeutic deeper into the skin due to their ability to sustain inertial cavitation activity throughout ultrasound exposure. This phenomenon has been shown in other studies to improve molecular transport in a gel [13], and also the transport of drugs into tissue [35].

*In vivo* testing of the ultrasound assisted transdermal delivery system has shown that delivery dose of 1  $\mu\text{g}$  can be achieved to murine skin in a 90 s treatment, without the use of chemical penetration enhancers, and that skin integrity is preserved, in stark contrast to when chemical penetration enhancers such as SDS are used. Furthermore, the long term immune response study demonstrated that a detectable level of OVA specific antibodies were detected in the mouse serum in response to an initial dose + booster treatment of ultrasound/NC assisted transdermal vaccination. Following the booster treatment, the ultrasound/NC assisted transdermal vaccination system outperformed the chemical penetration enhancers in terms of eliciting a limited but specific anti-OVA response. However, it is clear that this approach is still dramatically less effective than direct injection which provides guaranteed delivery of the dose in its entirety. Efforts are now focused on optimising gel formulation and ultrasound exposure parameters so that greater delivery and more robust responses can be achieved. It is hoped that such optimisation will help the field of transdermal vaccination progress so that reliable and robust needle free vaccination can be achieved.

Supplementary data to this article can be found online at <http://dx.doi.org/10.1016/j.jconrel.2016.07.016>.

#### Acknowledgements

The authors wish to thank Dr. Shaoyang Ye for his assistance with operation of the MPM, and gratefully acknowledge the financial support of the RCUK Digital Economy Programme (RCUK Digital Economy Programme grant number EP/G036861/1), the Oxford Martin School, and The Oxford Centre for Drug Delivery Devices (OXCD3) supported by a programme grant from the UK's Engineering and Physical Sciences Research Council (EP/L024012/1).

#### References

- [1] Safety of Injections Global Facts and Figures, World Health Organisation, 2004.
- [2] E.L. Giudice, J.D. Campbell, Needle-free vaccine delivery, *Adv. Drug Deliv. Rev.* 58 (2006) 68–89.
- [3] D.K. Mishra, V. Dhote, P.K. Mishra, Transdermal immunization: biological framework and translational perspectives, *Expert Opin. Drug Deliv.* 10 (2013) 183–200.
- [4] M.R. Prausnitz, R. Langer, Transdermal drug delivery, *Nat. Biotechnol.* 26 (2008) 1261–1268.
- [5] M.T.S. Lin, L. Pulkkinen, J. Uitto, K. Yoon, The gene gun: current applications in cutaneous gene therapy, *Int. J. Dermatol.* 39 (2000) 161–170.
- [6] Y.-C. Kim, J.-H. Park, M.R. Prausnitz, Microneedles for drug and vaccine delivery, *Adv. Drug Deliv. Rev.* 64 (2012) 1547–1568.
- [7] C.M. Schoellhammer, D. Blankschtein, R. Langer, Skin permeabilization for transdermal drug delivery: recent advances and future prospects, *Expert Opin. Drug Deliv.* 11 (2014) 393–407.

- [8] S. Mitragotri, D. Blankschtein, R. Langer, Ultrasound-mediated transdermal protein delivery, *Science* 269 (1995) 850–853.
- [9] S. Mo, C.-C. Coussios, L. Seymour, R. Carlisle, Ultrasound-enhanced drug delivery for cancer, *Expert Opinion on Drug Delivery* 9 (2012) 1525–1538.
- [10] H.A.E. Benson, J.C. McElnay, R. Harland, Phonophoresis of lignocaine and prilocaine from Emla cream, *Int. J. Pharm.* 44 (1988) 65–69.
- [11] S. Mitragotri, J. Kost, Low-frequency sonophoresis: a noninvasive method of drug delivery and diagnostics, *Biotechnol. Prog.* 16 (2000) 488–492.
- [12] S.S.S. Lanke, C.S. Kolli, J.G. Strom, A.K. Banga, Enhanced transdermal delivery of low molecular weight heparin by barrier perturbation, *Int. J. Pharm.* 365 (2009) 26–33.
- [13] S. Bhatnagar, H. Schiffter, C.-C. Coussios, Exploitation of acoustic cavitation-induced microstreaming to enhance molecular transport, *J. Pharm. Sci.* 103 (2014) 1903–1912.
- [14] S.M. Graham, R.S. Myers, J. Choi, M. Bazan-Peregrino, L. Seymour, R. Carlisle, C.C. Coussios, Use of micro- and nano-sized inertial cavitation nuclei to trigger and map drug release from cavitation-sensitive liposomes, *J. Acoust. Soc. Am.* 134 (2013) 4050.
- [15] J.J. Kwan, R. Myers, C.M. Coviello, S.M. Graham, A.R. Shah, E. Stride, R.C. Carlisle, C.C. Coussios, Ultrasound-Propelled Nanocups for Drug Delivery, *Small* 11 (2015) 5305–5314.
- [16] J.J. Kwan, S. Graham, R. Myers, R. Carlisle, E. Stride, C.C. Coussios, Ultrasound-induced inertial cavitation from gas-stabilizing nanoparticles, *Phys. Rev. E* 92 (2015) 023019.
- [17] U. Jacobi, M. Kaiser, R. Toll, S. Mangelsdorf, H. Audring, N. Otberg, W. Sterry, J. Lademann, Porcine ear skin: an in vitro model for human skin, *Skin Res. Technol.* 13 (2007) 19–24.
- [18] J.H. Cantrell, R.E. Goans, R.L. Roswell, Acoustic impedance variations at burn-nonburn interfaces in porcine skin, *The Journal of the Acoustical Society of America* 64 (1978) 731–735.
- [19] C.M. Moran, N.L. Bush, J.C. Bamber, Ultrasonic propagation properties of excised human skin, *Ultrasound Med. Biol.* 21 (1995) 1177–1190.
- [20] S. Bhatnagar, Cavitation-Mediated Transdermal Vaccination by Ultrasound in: Department of Engineering Science, University of Oxford, Oxford, 2015 209.
- [21] S. Mitragotri, J. Kost, Transdermal delivery of heparin and low-molecular weight heparin using low-frequency ultrasound, *Pharm. Res.* 18 (2001) 1151–1156.
- [22] A. Tezel, A. Sens, J. Tuchscherer, S. Mitragotri, Frequency dependence of sonophoresis, *Pharm. Res.* 18 (2001) 1694–1700.
- [23] A. Tezel, S. Paliwal, Z. Shen, S. Mitragotri, Low-frequency ultrasound as a transcutaneous immunization adjuvant, *Vaccine* 23 (2005) 3800–3807.
- [24] I. Som, K. Bhatia, M. Yasir, Status of surfactants as penetration enhancers in transdermal drug delivery, *J. Pharm. Bioall. Sci.* 4 (2012) 2.
- [25] H. Tang, C.C. Wang, D. Blankschtein, R. Langer, An investigation of the role of cavitation in low-frequency ultrasound-mediated transdermal drug transport, *Pharm. Res.* 19 (2002) 1160–1169.
- [26] A. Tezel, A. Sens, S. Mitragotri, Investigations of the role of cavitation in low-frequency sonophoresis using acoustic spectroscopy, *J. Pharm. Sci.* 91 (2002) 444–453.
- [27] K. König, K. Schenke-Layland, I. Riemann, U.A. Stock, Multiphoton autofluorescence imaging of intratissue elastic fibers, *Biomaterials* 26 (2005) 495–500.
- [28] M.J. Koehler, T. Vogel, P. Elsner, K. König, R. Bückle, M. Kaatz, In vivo measurement of the human epidermal thickness in different localizations by multiphoton laser tomography, *Skin Res. Technol.* 16 (2010) 259–264.
- [29] J. Matriano, M. Cormier, J. Johnson, W. Young, M. Buttery, K. Nyam, P. Daddona, Macroflux® microprojection array patch technology: a new and efficient approach for intracutaneous immunization, *Pharm. Res.* 19 (2002) 63–70.
- [30] J.F. Wang, M.E. Olson, C.R. Reno, W. Kulyk, J.B. Wright, D.A. Hart, Molecular and cell biology of skin wound healing in a pig model, *Connect. Tissue Res.* 41 (2000) 195–211.
- [31] H.A.E. Benson, J.C. McElnay, R. Harland, Use of ultrasound to enhance percutaneous absorption of benzydamine, *Phys. Ther.* 69 (1989) 113–118.
- [32] A. Boucaud, J. Montharu, L. Machet, B. Arbeille, M.C. Machet, F. Patat, L. Vaillant, Clinical, histologic, and electron microscopy study of skin exposed to low-frequency ultrasound, *Anat. Rec.* 264 (2001) 114–119.
- [33] A. Dahlan, H.O. Alpar, P. Stickings, D. Sesardic, S. Murdan, Transcutaneous immunisation assisted by low-frequency ultrasound, *Int. J. Pharm.* 368 (2009) 123–128.
- [34] J.t. Kushner, D. Blankschtein, R. Langer, Evaluation of the porosity, the tortuosity, and the hindrance factor for the transdermal delivery of hydrophilic permeants in the context of the aqueous pore pathway hypothesis using dual-radiolabeled permeability experiments, *J. Pharm. Sci.* 96 (2007) 3263–3282.
- [35] S.M. Graham, R. Carlisle, J.J. Choi, M. Stevenson, A.R. Shah, R.S. Myers, K. Fisher, M.-B. Peregrino, L. Seymour, C.C. Coussios, Inertial cavitation to non-invasively trigger and monitor intratumoral release of drug from intravenously delivered liposomes, *J. Control. Release* 178 (2014) 101–107.